# Regulation of outside-in signaling and affinity by the $\beta_2$ I domain of integrin $\alpha_L\beta_2$

JianFeng Chen*†, Wei Yang*, Minsoo Kim‡, Christopher V. Carman, and Timothy A. Springer§

CBR Institute for Biomedical Research and Department of Pathology, Harvard Medical School, 200 Longwood Avenue, Boston, MA 02115

Contributed by Timothy A. Springer, July 6, 2006

**The adhesiveness of integrin $\alpha_L\beta_2$ is modulated by divalent cations. We mutated three metal ion-binding sites in the $\beta_2$ I domain. The metal ion-dependent adhesion site (MIDAS) and the ligand-induced metal-binding site are required for ligand binding and sufficient for synergism between $Ca^{2+}$ and $Mg^{2+}$. Adjacent to MIDAS (ADMIDAS) mutants are constitutively active but remain bent, with poor exposure of a $\beta_2$ stalk region epitope. Fluorescence resonance energy transfer between fluorescent protein-fused $\alpha_L$ and $\beta_2$ cytoplasmic domains showed that ADMIDAS mutation abrogated ligand binding-induced spatial separation of cytoplasmic domains. Furthermore, ADMIDAS mutation abolished spreading on ligand-bearing substrates. Thus, $\beta_2$ I domain metal ion-binding sites regulate $\alpha_L$ I domain affinity, and the ADMIDAS is required for outside-in signaling.**

lymphocyte function-associated antigen-1 | CD11a/CD18 | adhesion

Integrins are $\alpha/\beta$ heterodimeric metalloproteins, the ligand-binding function of which depends on the interplay of $Ca^{2+}$, $Mg^{2+}$, and $Mn^{2+}$ ions. The liganded crystal structures of $\alpha_{IIb}\beta_3$ and $\alpha_V\beta_3$ reveal a striking linear cluster of three divalent cation-binding sites in the $\beta$ I domain (1, 2). The metal ion-dependent adhesion site (MIDAS) is at the center of the cluster. The outer two sites are known as the ligand-induced metal-binding site (LIMBS) and the adjacent to MIDAS (ADMIDAS) site. Work with integrins that lack $\alpha$ I domains ($\alpha_4\beta_7$ and $\alpha_5\beta_1$) has shown that the LIMBS and ADMIDAS modulate binding of ligand to the MIDAS (3–5).

Integrins adopt a bent, compact conformation in their low-affinity state and an extended conformation in the high-affinity state (1, 2, 6–10). Furthermore, ligand binding induces the extension of the extracellular domain and a movement at the $\beta$ I domain–hybrid domain interface (1, 9, 10). The $\beta$ I domain is inserted in the hybrid domain (i.e., it is connected at both its N and C terminus to the hybrid domain). Crystal structures of integrin $\alpha_{IIb}\beta_3$ in the liganded, high-affinity conformation reveal that the C-terminal $\alpha$7-helix of the $\beta$ I domain moves axially toward the hybrid domain, causing the $\beta$ hybrid domain to pivot about its other connection and to swing outward by 62°, away from the $\alpha$-subunit (1). Movement of the $\alpha$7-helix is linked to that of the adjacent $\alpha$1-helix and to movements of the preceding $\beta$6-$\alpha$7 and $\beta$1-$\alpha$1 loops, which form important coordinations at the MIDAS and ADMIDAS. Thus, the $\alpha$7-helix is a key allosteric link between the ligand-binding site in the $\beta$ I domain and the hybrid domain. Accompanying integrin extension, the cytoplasmic and transmembrane domains separate, which enables bidirectional signal transmission across the plasma membrane (11).

Half of the vertebrate integrin $\alpha$-subunits contain $\alpha$ I domains, which mediate ligand binding (6, 8, 12). Here, we examine in integrins with $\alpha$ I domains whether the $\beta$ I domain LIMBS and ADMIDAS modulate ligand binding as they do in integrins where the $\beta$ I domain directly participates in ligand binding. Furthermore, we find that the ADMIDAS is required to couple ligand binding with $\alpha_L$ and $\beta_2$ cytoplasmic domain separation and outside-in signaling.

**Table 1. Expression of $\alpha_L\beta_2$ mutants**

| Mutated site | Mutated residue | | Expression, % WT |
|---|---|---|---|
| | $\beta_2$ residue | $\beta_3$ residue | |
| WT | — | — | 100 ± 11 |
| MIDAS | Ser-114 | Ser-121 | 60 ± 9 |
| ADMIDAS | Asp-119 | Asp-126 | 87 ± 14 |
| ADMIDAS | Asp-120 | Asp-127 | 92 ± 20 |
| LIMBS | Asn-207 | Asn-215 | 98 ± 18 |
| LIMBS | Asp-209 | Asp-217 | 98 ± 15 |

All mutations were to Ala. Integrin $\alpha_L\beta_2$ cell surface expression in 293T transient transfectants was determined by TS2/4 mAb staining and immunofluorescence flow cytometry. The data are mutant-specific fluorescence intensity as a percentage of WT-specific fluorescence intensity (mean ± SD from four independent experiments). —, not applicable.

## Results

**Design and Cell Surface Expression of Mutant $\alpha_L\beta_2$ Integrins.** To investigate the function of the $\beta$ I domain LIMBS, MIDAS, and ADMIDAS (LMA) sites in regulating the ligand-binding affinity of $\alpha_L\beta_2$, representative primary coordinating residues of each metal ion-binding site were mutated to Ala (Table 1). The $\beta_3$ and $\beta_2$ I domains are highly conserved, with 50.4% amino acid sequence identity. All residues with side chains coordinating to LMA metal ions are identical (Fig. 1*A*). Because of the high identity in sequence and absolute identity in coordinating side chains, we assume that the $\beta_3$ I domain structure is an excellent model for understanding the effect of $\beta_2$ LMA mutations. Immunofluorescence flow cytometry with TS2/4, a mAb that recognizes the $\alpha_L$-subunit $\beta$-propeller domain only when it is associated with $\beta_2$-subunit I domain (13), demonstrated that the $\beta_2$ AMIDAS and LIMBS mutants were expressed at WT levels in 293T transfectants and that the $\beta_2$ MIDAS mutant was expressed at 60% of WT levels (Table 1).

**Regulation of $\alpha_L\beta_2$ Adhesion by Divalent Cations.** The binding in different divalent cations of soluble human intercellular adhesion molecule-1 (ICAM-1)–IgA Fc fusion protein (ICAM-1–Fc$\alpha$) complexed with FITC-anti-IgA to $\alpha_L\beta_2$ 293T transfectants was measured by immunofluorescence flow cytometry. There was little binding of ICAM-1–Fc$\alpha$ complexes to cells expressing

Conflict of interest statement: No conflicts declared.

Abbreviations: MIDAS, metal ion-dependent adhesion site; ADMIDAS, adjacent to MIDAS; LIMBS, ligand-induced metal-binding site; LMA, LIMBS, MIDAS, and ADMIDAS; ICAM-1, intercellular adhesion molecule-1; mCFP, monomeric mutant of cyan fluorescent protein; mYFP, monomeric mutant of yellow fluorescent protein.

*J.C. and W.Y. contributed equally to this work.

†Present address: Institute of Biochemistry and Cell Biology, Chinese Academy of Sciences, Shanghai 200031, China.

‡Present address: Division of Surgical Research, Brown University School of Medicine, Rhode Island Hospital, 593 Eddy Street, Middlehouse 207, Providence, RI 02903.

§To whom correspondence should be addressed. E-mail: springeroffice@cbr.med.harvard.edu.





www.pnas.org/cgi/doi/10.1073/pnas.0605666103

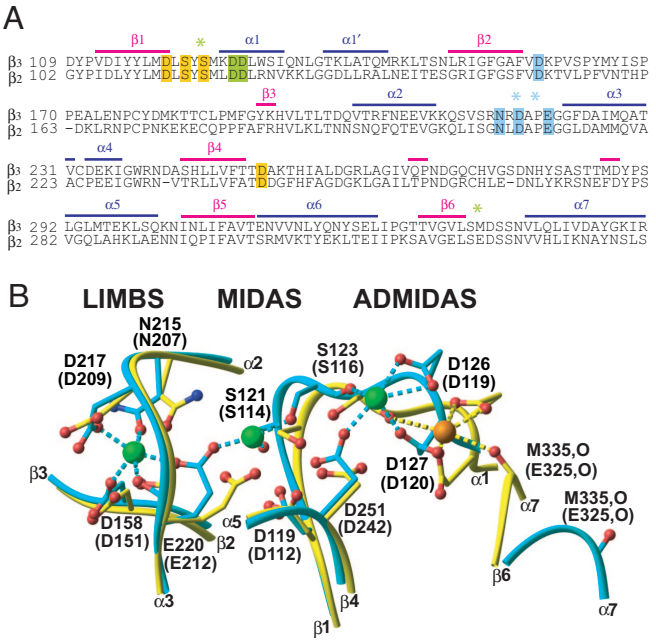


**Fig. 1.** The $\beta$I domain metal-binding sites. (*A*) Sequence alignment of human integrin $\beta_3$ and $\beta_2$ I domains. Residues with metal-coordinating side-chain oxygen atoms are highlighted, and residues with metal-coordinating backbone carbonyl oxygen atoms are asterisked. Highlights and asterisks are color-coded as follows: orange, MIDAS; green, ADMIDAS; cyan, LIMBS. (*B*) The linear cluster of $\beta$ I domain metal-binding sites. The sites are shown in the liganded, open $\alpha_{IIb}\beta_3$ structure (cyan) (1) and the unliganded, closed $\alpha_V\beta_3$ structure in $Ca^{2+}$ (yellow) (41), superimposed by using the $\beta$ I domain. Metal ions are shown as large green and orange spheres for open and closed structures, respectively. Metal-coordinating side chains and backbone carbonyl groups are shown, with N and O atoms in blue and red, respectively. Residues are labeled for $\beta_3$ and are shown in parentheses for $\beta_2$.

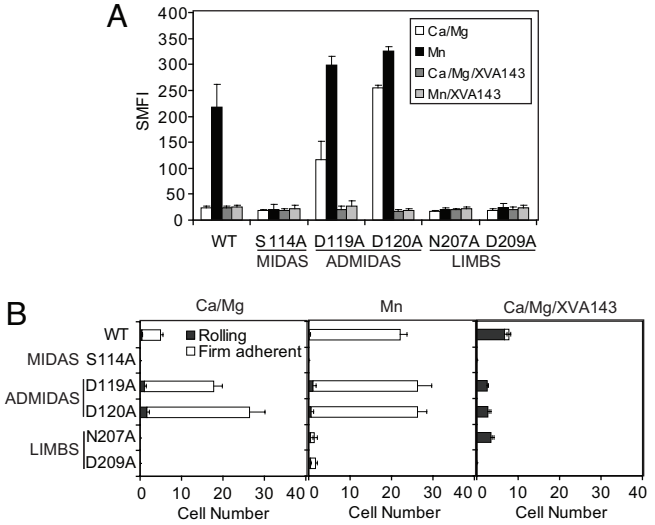


**Fig. 2.** Integrin affinity regulation by mutations of the $\beta_2$ I domain metal ion-binding sites. (*A*) Binding of ICAM-1–Fc$\alpha$ to 293T cell transient transfectants. Binding was assayed in Hepes/NaCl/glucose/BSA (20 mM Hepes, pH 7.5/140 mM NaCl/2 mg/ml glucose/1% BSA) supplemented with 1 mM $CaCl_2$/1 mM $MgCl_2$, 1 mM $MnCl_2$, or 1 mM $MnCl_2$/1 $\mu$M XVA143 as indicated at room temperature. The specific mean fluorescence intensity was normalized by dividing by the ratio of mutant/WT TS2/4 mAb-specific mean fluorescence intensity. (*B*) The adhesive modality of $\alpha_L\beta_2$ and resistance to detachment in shear flow. Rolling and firmly adherent WT and mutant $\alpha_L\beta_2$ 293T transient transfectants were enumerated in 1 mM $CaCl_2$/1 mM $MgCl_2$, 1 mM $MnCl_2$, or 1 mM $CaCl_2$/1 mM $MgCl_2$ plus 1 $\mu$M XVA134 at incremental wall shear stresses. Results at 1, 2, 4, and 8 dyne·cm$^{-2}$ were very similar and are averaged together. Error bars show the SD of three independent experiments.

WT $\alpha_L\beta_2$ in 1 mM $Ca^{2+}$/1 mM $Mg^{2+}$. ICAM-1–Fc$\alpha$ binding was greatly enhanced by replacement of 1 mM $Ca^{2+}$/1 mM $Mg^{2+}$ with 1 mM $Mn^{2+}$ (Fig. 2*A*). Similar results were obtained in parallel plate shear flow adhesion assays with human ICAM-1–$IgG_1$ Fc fusion protein (ICAM-1–Fc$\gamma$) incorporated on the lower wall of the flow chamber (Fig. 2*B*). Cells were allowed to accumulate on ICAM-1–Fc$\gamma$ at a wall shear stress of 0.3 dyne·cm$^{-2}$ (1 dyne = 10 $\mu$N) for 30 s. Then, the wall shear stress was incrementally increased every 10 s, and the velocity of the cells remaining bound at each increment was determined and used to enumerate rolling and firmly adherent cells. Compared with 1 mM $Ca^{2+}$/1 mM $Mg^{2+}$, 1 mM $Mn^{2+}$ greatly increased the number of WT firmly adherent cells (Fig. 2*B*).

**Regulation of Adhesion by $\beta_2$ I Domain LMA Sites.** The $\beta_2$ MIDAS mutation, S114A, completely abolished $\alpha_L\beta_2$ ligand binding under all conditions (Fig. 2). Relative to WT, the two ADMIDAS mutations, D119A and D120A, strikingly enhanced multimeric ICAM-1–Fc$\alpha$ binding in the presence of 1 mM $Ca^{2+}$/$Mg^{2+}$ (Fig. 2*A*). Similarly, the ADMIDAS mutations greatly enhanced accumulation in shear flow in the presence of 1 mM $Ca^{2+}$/$Mg^{2+}$ (Fig. 2*B*). In contrast, the two LIMBS mutations, N207A and D209A, abolished adhesion in shear flow in 1 mM $Ca^{2+}$/$Mg^{2+}$, although they mediated very weak adhesion in the presence of 1 mM $Mn^{2+}$ (Fig. 2*B*). Adhesion to ICAM-1 in the above two assays is mediated by the $\alpha_L$ I domain, as previously shown (14, 15). The above results demonstrate that $\alpha_L$ I domain-mediated ligand binding to ICAM-1 is regulated by the $\beta_2$ I domain LMA sites.

**The Effect of $\alpha_L\beta_2$ Small Molecule Antagonist XVA143.** XVA143 is an $\alpha_L\beta_2$ allosteric antagonist that binds to the $\beta_2$ I domain MIDAS and blocks transmission of activation signals to the $\alpha_L$ I domain (14, 16, 17). In both $Ca^{2+}$/$Mg^{2+}$ and $Mn^{2+}$, XVA143 (1 $\mu$M) completely inhibited multimeric ICAM-1–Fc$\alpha$ binding to WT $\alpha_L\beta_2$ and the ADMIDAS mutants, D119A and D120A (Fig. 2*A*). XVA143 somewhat increased the number of WT cells that accumulated in shear flow and greatly increased the number of rolling cells and decreased the number of firmly adherent cells as described in ref. 14 (Fig. 2*B*). The firm adhesion induced by the ADMIDAS mutants in $Ca^{2+}$/$Mg^{2+}$ was completely blocked by XVA143 (Fig. 2*B*). These results demonstrate that, as expected, and as previously demonstrated for regulation of adhesiveness by $Mn^{2+}$ (14, 18), signal transmission from the $\beta_2$ I domain to the $\alpha_L$ I domain is required for activation of adhesiveness by the ADMIDAS mutants.

**Positive and Negative Regulation by Low and High $Ca^{2+}$ Concentrations.** For most integrins, $Ca^{2+}$ has both positive and negative regulatory effects. Low (≈0.1 mM) concentrations of $Ca^{2+}$ augment adhesion at suboptimal (≈0.1 mM) $Mg^{2+}$ concentrations, whereas higher (1–10 mM) concentrations of $Ca^{2+}$ inhibit adhesion at optimal (≈1 mM) $Mg^{2+}$ concentrations (3, 19–21). The ADMIDAS mutants allowed us to study these effects under conditions in which basal adhesiveness was augmented and the contribution of metal ion binding to the ADMIDAS could be ruled out. At a range of wall shear stresses, little accumulation on ICAM-1 substrates of ADMIDAS mutant D120A was seen in 50 $\mu$M $Ca^{2+}$ or 50 $\mu$M $Mg^{2+}$, whereas the combination of 50 $\mu$M $Ca^{2+}$ and 50 $\mu$M $Mg^{2+}$ synergistically promoted strong adhesiveness (Fig. 3*A*). Therefore, the $\beta_2$ I LIMBS and MIDAS are sufficient for synergism between $Ca^{2+}$ and $Mg^{2+}$.

Accumulation in shear flow on ICAM-1 substrates of WT $\alpha_L\beta_2$ transfectants in 1 mM $Mn^{2+}$ was greatly decreased by

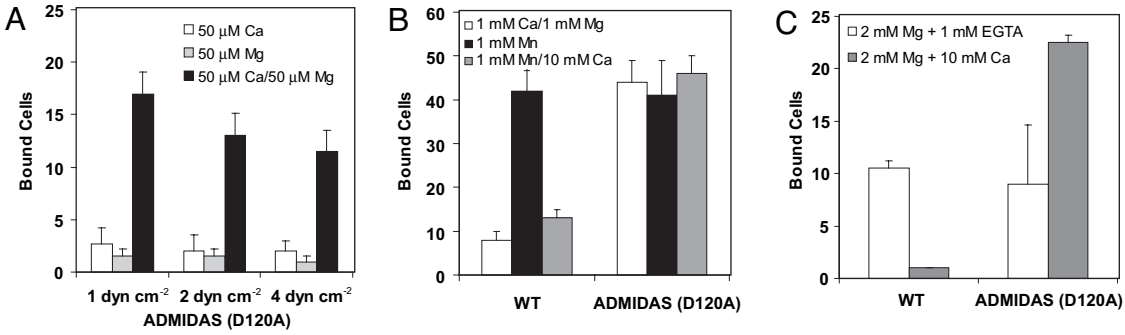


**Fig. 3.** Positive and negative regulation of $\alpha_L\beta_2$ by $Ca^{2+}$. (*A*) Synergistic effect of low concentrations of $Ca^{2+}$ and $Mg^{2+}$ on the adhesion of $\alpha_L\beta_2$ D120A 293T transfectants on ICAM-1. The number of adherent cells was measured in the indicated divalent cations at different wall shear stress. (*B* and *C*) Effect of 10 mM $Ca^{2+}$ on the adhesion of $\alpha_L\beta_2$ 293T transfectants to ICAM-1. Adherent cells were enumerated in the indicated divalent cations at the wall shear stress of 2 dyne·cm$^{-2}$. The data show mean ± SD from three independent experiments.

addition of 10 mM $Ca^{2+}$ (Fig. 3*B*). In contrast, 10 mM $Ca^{2+}$ had no inhibitory effect on the accumulation of the $\alpha_L\beta_2$ ADMIDAS mutant. Similarly, high concentrations of $Ca^{2+}$ inhibited the $Mg^{2+}$-promoted adhesion of WT $\alpha_L\beta_2$ transfectants but not $\alpha_L\beta_2$ ADMIDAS transfectants (Fig. 3*C*). Indeed, $Ca^{2+}$ enhanced adhesiveness by the ADMIDAS mutant (Fig. 3*C*), consistent with the synergism seen in Fig. 3*A*. These results strongly suggest that the $\beta_2$ I domain ADMIDAS is responsible for inhibition of $\alpha_L\beta_2$ adhesiveness by high $Ca^{2+}$ concentrations.

**Integrin Conformational Changes Induced by $\beta$ I Domain LMA Mutations.** To study the effect on integrin conformation by the $\beta_2$ I domain LMA mutations, the exposure of epitopes recognized by two anti-$\beta_2$ activation-dependent mAbs was measured. The extended conformation of the $\beta_2$-subunit is reported by the mAb KIM127, which maps to species-specific residues in the integrin EGF2 domain of integrin $\beta_2$ subunit that are buried in the headpiece–tailpiece interface in the bent integrin conformation and exposed in the extended conformation (7, 22). The active conformation of the $\beta_2$ I domain is detected by mAb m24, which recognizes the species-specific residues Arg-122 in the $\alpha$1-helix and Glu-175 in the specificity-determining loop of the $\beta_2$ I domain (23–25).

KIM127 bound poorly to WT $\alpha_L\beta_2$ transfectants in the presence of $Ca^{2+}/Mg^{2+}$ (Fig. 4*A*). Activation by $Mn^{2+}$ or $Mn^{2+}$ plus a soluble, monomeric ectodomain fragment of ICAM-1 containing Ig superfamily domains 1–5 (sICAM-1) greatly enhanced the KIM127 binding to WT $\alpha_L\beta_2$ (Fig. 4*A*). Binding of KIM127 was highest in XVA143. The results with WT $\alpha_L\beta_2$ and the m24 epitope were similar, except that binding in XVA143 was lower than in $Mn^{2+}$ and $Mn^{2+}$/sICAM-1 (Fig. 4*A*). Neither antibody bound to the S114A MIDAS mutant. Binding of KIM127 and m24 antibodies to the D120A ADMIDAS mutant was abolished in $Mn^{2+}$ and $Mn^{2+}$/sICAM-1 and only slightly enhanced (if at all) by XVA143 (Fig. 4*A*). In contrast, D119A transfectants showed low binding to KIM127 antibody, with little influence by divalent cations and sICAM-1, and WT level binding in XVA143 (Fig. 4*A*). The D119A mutant showed $Mn^{2+}$-augmented binding to m24 that was below WT levels and augmentation by XVA143 that was near WT level. The LIMBS mutants N207A and D209A showed greatly decreased KIM127 and m24 binding compared with WT in $Mn^{2+}$ and $Mn^{2+}$/sICAM-1, and the N207A mutant showed near WT levels of binding in XVA143.

The above experiments demonstrate that the KIM127 epitope is largely masked in $Ca^{2+}/Mg^{2+}$, $Mn^{2+}$, and $Mn^{2+}$/sICAM-1 in the ADMIDAS and LIMBS mutants. Thus, despite activation of ligand binding by the ADMIDAS mutations, and in contrast to activated WT $\alpha_L\beta_2$, the ADMIDAS mutants remain in the bent conformation. The complete inhibition by XVA143 of firm adhesion of the ADMIDAS mutants in Fig. 2*B* acts as a positive control for the effects of XVA143 on the KIM127 epitope in Fig. 4*A*. Thus, we may conclude that ADMIDAS mutant D120A blocks KIM127 epitope exposure induced by $Mn^{2+}$, $Mn^{2+}$/sICAM-1, and XVA143 and that the D119A ADMIDAS mutant blocks exposure induced by $Mn^{2+}$ and $Mn^{2+}$/sICAM-1 but not exposure induced by XVA143. The results with m24 in the above experiments must be interpreted with caution, because m24 binds to species-specific residues that lie on either side of the

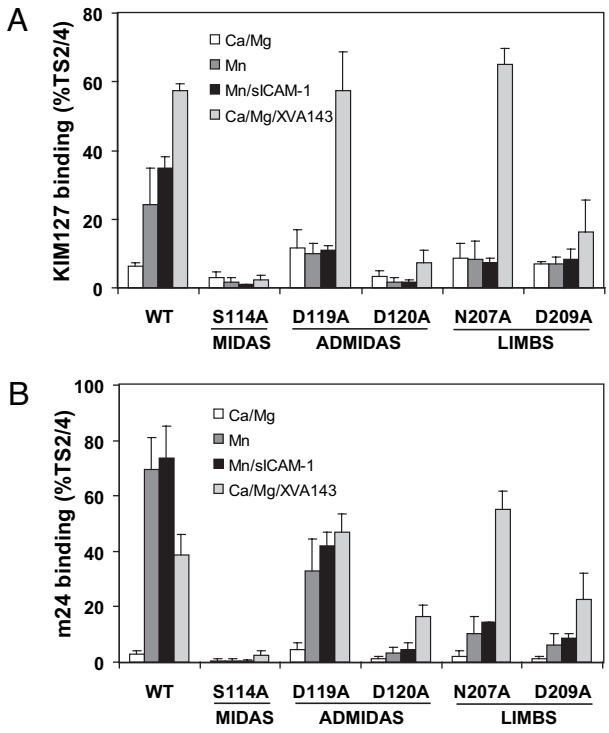


**Fig. 4.** Effect of $\beta$ I domain metal ion-binding site mutations and XVA143 on integrin conformation. The epitope exposure of $\beta_2$ activation-dependent mAbs KIM127 (*A*) and m24 (*B*) was measured. WT and mutant 293T transient transfectants in medium containing 1 mM $CaCl_2$/1 mM $MgCl_2$, 1 mM $MnCl_2$, or 1 mM $MnCl_2$/100 $\mu$g/ml sICAM-1 were stained with KIM127 or m24 mAbs and subjected to immunofluorescence flow cytometry. Expression of the activation-insensitive mAb TS2/4 was not affected by $MnCl_2$ and sICAM-1. Data show specific mean fluorescence intensity as a percentage of TS2/4-specific mean fluorescence intensity, and error bars represent the SD of three independent experiments.

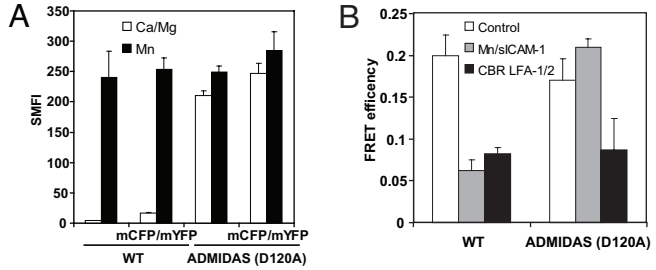


**Fig. 5.** Ligand binding to activated $\alpha_L$-mCFP/$\beta_2$-mYFP causes spatial separation of the cytoplasmic domains of WT $\alpha_L\beta_2$ but not the ADMIDAS mutant. (*A*) The C-terminal mCFP and mYFP fusions have no effect on the function of $\alpha_L\beta_2$. The binding of ICAM-1–Fc$\alpha$ complexes to 293T cell transfectants was measured in the presence of 1 mM $CaCl_2$/1 mM $MgCl_2$ and 1 mM $MnCl_2$. Error bars show the SD of three independent experiments. (*B*) Intersubunit FRET efficiency was measured in K562 stable transfectants expressing WT and D120A ADMIDAS mutant $\alpha_L$-mCFP/$\beta_2$-mYFP. Cells were treated in L15 medium supplemented with 2.5% FCS (control), 1 mM $MnCl_2$ plus 100 $\mu$g/ml sICAM-1 (Mn/sICAM-1), or 20 $\mu$g/ml $\alpha_L\beta_2$-activating mAb CBR LFA-1/2 (CBR LFA-1/2). Data show mean ± SD for 5–10 cells.

LMA sites. Thus, the LMA sites may comprise part of the m24 epitope, and mutations in these sites, the presence of $Mn^{2+}$, and binding of XVA143 may directly affect the m24 epitope.

**The ADMIDAS Is Essential for Coupling Integrin Ligand Binding and Cytoplasmic Domain Separation.** The lack of basal KIM127 exposure in the ADMIDAS mutants suggested that the ADMIDAS may not only regulate ligand binding but also couple ligand binding to global integrin conformation and to signaling by integrin cytoplasmic domains. We investigated this possibility with the ADMIDAS mutant that shows the least basal KIM127 epitope exposure, D120A. Monomeric mutants of cyan fluorescent protein (mCFP) and yellow fluorescent protein (mYFP) were fused to the C termini of integrin $\alpha_L$- and $\beta_2$- subunits, respectively, as previously described for WT $\alpha_L\beta_2$ (11). The addition of C-terminal mCFP and mYFP did not affect ligand binding by WT or D120A transfectants (Fig. 5*A*).

Significant FRET between mCFP and mYFP was seen with WT $\alpha_L$-mCFP/$\beta_2$-mYFP transfectants in L15 medium, which contains $Ca^{2+}$ and $Mg^{2+}$ (Fig. 5*B*, control). Activation with 1 mM $Mn^{2+}$ and 100 $\mu$g/ml sICAM-1 greatly decreased FRET (Fig. 5*B*), as described in ref. 11. In contrast, 1 mM $Mn^{2+}$ and 100 $\mu$g/ml sICAM-1 did not decrease FRET of the ADMIDAS D120A mutant, despite evidence that it is more active in ligand binding than WT in $Mn^{2+}$ (Fig. 2). As a positive control, we used CBR LFA-1/2, a mAb that binds to the $\beta_2$ integrin EGF3 domain, activates ligand binding, and induces integrin extension (7, 22). CBR LFA-1/2 decreased FRET of WT $\alpha_L\beta_2$, as reported in ref. 11, and decreased FRET of the D120A mutant $\alpha_L\beta_2$ to a similar level (Fig. 5*B*). These results demonstrate that the D120A ADMIDAS mutation disrupts outside-in signaling in $\alpha_L\beta_2$.

**ADMIDAS Mutation Blocks $\alpha_L\beta_2$-Mediated Cell Spreading.** To further examine the requirement of the $\beta_2$ I domain ADMIDAS for outside-in signaling, $\alpha_L\beta_2$-mediated cell spreading was studied. Transfectants expressing WT $\alpha_L\beta_2$ spread on ICAM-1 substrates (Fig. 6*A*). Interference-reflection microscopy (IRM) showed an extensive area of close cell–substrate contact (Fig. 6*A*). In contrast, the $\alpha_L\beta_2$ ADMIDAS mutant transfectants did not spread on ICAM-1 (Fig. 6*A*) and showed the same area of projection on the substrate as cells in suspension (Fig. 6*B*). IRM confirmed close contact of the ADMIDAS mutant transfectants with the substrate, in agreement with their adhesiveness, but the area of contact was much smaller than for WT transfectants and remained round, in contrast to the irregular shape of the cell–substrate contacts of the WT transfectants. These results demonstrate that the $\beta_2$ I domain ADMIDAS mutation abolishes $\alpha_L\beta_2$-mediated cell spreading.

## Discussion

We have examined the role of the LMA sites in the $\beta$ I domain of the $\beta_2$ subunit in regulating ligand binding, integrin extension, and outside-in signaling. As previously demonstrated (26), mutation of the $\beta_2$ I MIDAS abolishes ligand binding by $\alpha_L\beta_2$. Mutation of $\alpha_L$ Glu-310 (27) and the corresponding residue in $\alpha_M$ (28) shows that this residue, which follows the $\alpha$ I domain C-terminal helix and is invariant in I domain-containing integrins, is required for I domain activation. Cross-linking of this residue to loops surrounding the MIDAS activates ligand binding by $\alpha_L\beta_2$ (18) and supports the proposal that, when activated, the $\beta_2$ I domain MIDAS coordinates Glu-310 of the $\alpha_L$ I domain and activates the $\alpha_L$ I domain by exerting a downward pull on its $\alpha$7-helix (18, 28). According to this model, $\beta$ I domains of integrins that lack or contain $\alpha$ I domains function similarly and bind to extrinsic ligands or an intrinsic ligand, respectively (e.g., Glu-310 in $\alpha_L$).

Mutation of the $\beta_2$ I domain LIMBS residues almost completely eliminated multivalent soluble ligand binding and adhesion in shear flow. The presence of the $\beta_2$ LIMBS and MIDAS sites is sufficient for synergy between 50 $\mu$M $Ca^{2+}$ and 50 $\mu$M $Mg^{2+}$ in supporting ligand binding, as shown with an ADMIDAS mutant. In a structure of the $\alpha_{IIb}\beta_3$ headpiece determined in the presence of $Ca^{2+}$ and $Mg^{2+}$, $Ca^{2+}$ and $Mg^{2+}$ ions were assigned at the LIMBS and MIDAS, respectively (1). Assignment was based on the presence of two carbonyl oxygen coordinations at

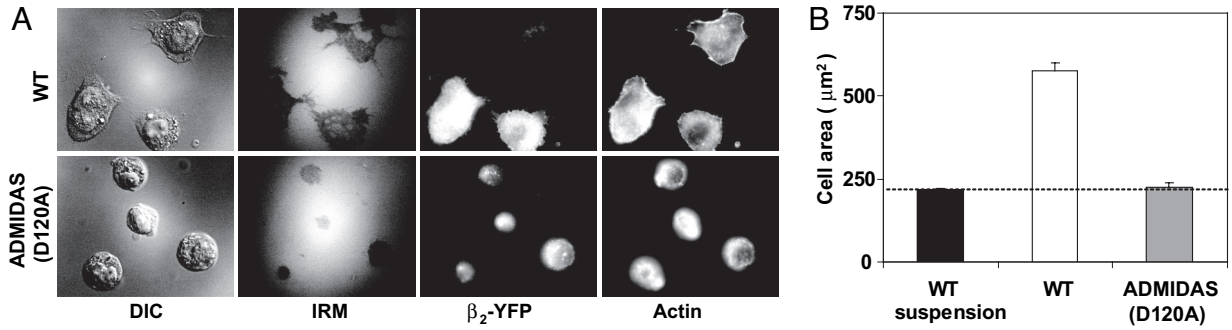


**Fig. 6.** ADMIDAS mutation blocks $\alpha_L\beta_2$-mediated cell spreading. (*A*) Differential interference contrast and interference-reflection microscopy images of $\alpha_L\beta_2$-expressing 293T transient transfectants after adhering at 37°C to immobilized human ICAM-1–Fc$\gamma$ (for 2 h) in DMEM without FCS. The localization of the yellow fluorescent protein-fused $\beta_2$-subunit and actin stained with phalloidin is also shown. The images are representatives from one of three independent experiments. (*B*) Cell area (projection on the substrate) was measured as described in *Materials and Methods*.

the LIMBS and none at the MIDAS, and the far greater propensity of $Ca^{2+}$ than $Mg^{2+}$ for carbonyl oxygen coordination (29). Synergy between LIMBS and MIDAS is readily explicable, based on the high-affinity $\alpha_{IIb}\beta_3$ headpiece structure, which shows that the Glu-220 side chain coordinates with one of its oxygens to the LIMBS $Ca^{2+}$ ion and with its other oxygen to the MIDAS $Mg^{2+}$ ion (Fig. 1*B*). Synergy between $Ca^{2+}$ and $Mg^{2+}$ is also seen for binding of ligands to ADMIDAS mutant integrins $\alpha_4\beta_7$ (3) and $\alpha_5\beta_1$ (5). LIMBS mutants abolish ligand binding to $\alpha_4\beta_7$ (3) and have previously been reported to abolish ligand binding to $\alpha_L\beta_2$ (25). These observations demonstrate the similar function of the LIMBS in regulation of ligand binding by integrins that lack and contain $\alpha$ I domains.

Mutation of the ADMIDAS activated ligand binding but abolished conformational linkage between the $\alpha_L$ I domain and the $\alpha_L$ and $\beta_2$ cytoplasmic domains, revealing the crucial role for the ADMIDAS in relaying allostery to cytoplasmic domains in integrins. The ADMIDAS mutations activated binding to soluble, multimeric ICAM-1 and to ICAM-1 substrates in shear flow. We did not see binding at levels above WT of the ADMIDAS mutants to ICAM-1 in static adhesion/washing assays (data not shown), which is in agreement with another report on D120A mutation (25). Assay-dependent differences may be explained by activation of ligand binding but not extension or cellular spreading by the ADMIDAS mutations; the shear flow LFA-1 adhesion assay used here is markedly more sensitive than adhesion assays in which cells are subjected to high and poorly defined shear during the wash step (15). Mutation of the ADMIDAS prevented inhibition of ICAM-1 binding by high 10 mM $Ca^{2+}$ concentrations and, as mentioned above, did not affect stimulation of adhesion by low $Ca^{2+}$ concentrations. These observations, together with the negative and positive regulatory effects of LIMBS and ADMIDAS mutations, respectively, suggest that the LIMBS and ADMIDAS are the sites for positive and negative regulation, respectively, of $\alpha_L\beta_2$ by $Ca^{2+}$. Similar observations on $\alpha_4\beta_7$ (3) and $\alpha_5\beta_1$ (5) further support similarity in function between $\beta$ I domains in integrins that lack and contain $\alpha$ I domains. Studies on ADMIDAS mutants in $\alpha_5\beta_1$ used $\alpha_5\beta_1$ headpiece or $\alpha_5\beta_1$ ectodomain fragments fused to Fc (5) and are somewhat difficult to compare with the assays on cell surface $\alpha_L\beta_2$ presented here, in part because the "WT" $\alpha_5\beta_1$ ectodomain Fc fusion is active, whereas WT cell surface $\alpha_L\beta_2$ is inactive. The observation that a $Mn^{2+}$-dependent increase in a hybrid domain activation-dependent epitope was blocked by ADMIDAS mutations in the $\alpha_5\beta_1$ headpiece–Fc fusion was interpreted as suggesting a function for the ADMIDAS in transmitting conformational change from the MIDAS to the hybrid domain (5) and is compatible with our results in full-length $\alpha_L\beta_2$. However, ADMIDAS mutation in $\alpha_5\beta_1$ inhibits ligand binding (5). This finding contrasts with results in $\alpha_4\beta_7$ and $\alpha_L\beta_2$ and may suggest a direct role in ligand binding for the ADMIDAS in $\alpha_5\beta_1$, in addition to a regulatory role.

Our most striking finding is that the ADMIDAS is required to link ligand binding to integrin extension, cytoplasmic domain separation, and cellular spreading on adhesive substrates. Despite activation of ligand binding by ADMIDAS mutation, exposure of the KIM127 epitope, which reports integrin extension, was markedly decreased in the D119A mutant and essentially absent in the D120A mutant. Structural studies in $\alpha_{IIb}\beta_3$ (1) and mutational studies in other integrins, including $\alpha_{IIb}\beta_3$, $\alpha_5\beta_1$, and $\alpha_L\beta_2$ (30–33), have shown the importance of the $\alpha$1-helix, $\beta$6-$\alpha$7 loop, and $\alpha$7-helix in allosteric communication between the $\beta$ I and hybrid domains. The ADMIDAS comprises residues in the $\alpha$1-helix and $\beta$6-$\alpha$7 loop (Fig. 1*B*). In the high-affinity, liganded integrin conformation, the $\alpha$1-helix straightens and moves laterally, displacing the $\beta$6-$\alpha$7 loop (Fig. 1*B*) and facilitating the downward, axial displacement of the $\alpha$7-helix that triggers hybrid domain swing-out (1). However, ligand binding can be dissociated from all of these rearrangements except those immediately in the ligand-binding site when hybrid domain swing-out is prevented by crystal lattice contacts (2). Similarly, our results suggest that ADMIDAS mutations facilitate shifts at the MIDAS of $\alpha$1-helix residues S114 and S116 toward the ligand-binding configuration and, at the same time, release structural constraints on the $\alpha$1-helix imposed by its $Ca^{2+}$-binding ADMIDAS residues, D119 and D120 (Fig. 1*B*), so that the more C-terminal portion of the $\alpha$1-helix and the $\beta$6-$\alpha$7 loop and $\alpha$7-helix can retain conformations similar to those in the low-affinity state.

Our study shows that the ADMIDAS is required for signal transmission all of the way to the integrin $\alpha$- and $\beta$-subunit cytoplasmic domains. FRET studies showed that, despite activation by ADMIDAS mutation of ligand binding, and in agreement with lack of integrin extension reported by the KIM127 antibody, the $\alpha$- and $\beta$-subunit cytoplasmic domains did not separate. Furthermore, high concentrations of soluble ICAM-1, which induced cytoplasmic domain separation by WT $\alpha_L\beta_2$, failed to do so with the ADMIDAS mutant. Perhaps most remarkably, despite adhesion to ICAM-1 substrates, the ADMIDAS mutant transfectants completely failed to spread, as shown by visualizing cells, $\alpha_L\beta_2$, the actin cytoskeleton, and regions of close contact with the substrate. Spreading is an active process that requires cooperative interactions between integrin cytoplasmic domains and cytoskeletal components and is one of the key "postligand-binding" or "outside-in signaling" events triggered by integrins. Thus, our results demonstrate that the ADMIDAS in the $\beta_2$ I domain not only is an important regulator of ligand binding by the $\alpha_L$ I domain but also is required to couple ligand binding to $\alpha_L$ and $\beta_2$ cytoplasmic domain separation and downstream signals that trigger cellular spreading on ligand-bearing substrates.

## Materials and Methods

**cDNA Construction and Expression.** The $\beta_2$ site-directed mutations were generated with the QuikChange site-directed mutagenesis system (Stratagene, La Jolla, CA). WT human $\beta_2$ cDNA in vector pcDNA3.1(+) (Invitrogen, Carlsbad, CA) was used as the template. All mutations were confirmed by DNA sequencing. The $\alpha_L\beta_2$ constructs used for FRET were exactly as described in ref. 11, except for introduction of the D120A mutation.

**Cells Lines and Antibodies.** Transient transfection of 293T and stable transfection of K562 cells were performed as described in refs. 11, 34, and 35. Activating mouse anti-human mAb CBR LFA-1/2 specific for $\beta_2$ is described in refs. 22 and 36. Activation-dependent mAbs KIM127 (37) and m24 (23, 24) were kindly provided by M. Robinson (Celltech, Slough, U.K.) and N. Hogg (Imperial Cancer Research Fund, London, U.K.), respectively. Mouse anti-human $\alpha_L$ mAb TS2/4 was used to measure the cell surface expression of $\alpha_L\beta_2$.

**Immunofluorescence Flow Cytometry.** Immunofluorescence flow cytometry was performed as described in ref. 35. mAbs were used as 10 $\mu$g/ml purified IgG. Binding of KIM127 to cells was in Hepes saline (20 mM Hepes, pH 7.5/150 mM NaCl) at 37°C, supplemented as indicated and detected by FITC-conjugated anti-mouse IgG (Pharmingen, San Jose, CA). Binding of other mAbs to cells was in Hepes saline at 4°C, supplemented as indicated and detected by FITC-anti-mouse IgG.

**Soluble ICAM-1.** Binding of soluble human ICAM-1-IgA Fc fusion protein (ICAM-1–Fc$\alpha$) (38) complexed with affinity-purified, FITC-conjugated anti-human IgA (Zymed, South San Francisco, CA) or phycoerythrin (PE)-conjugated anti-human IgA (Open Biosystems, Huntsville, AL) was measured by flow cytometry (16). PE-conjugated anti-human IgA was used for

$\alpha_L$-mCFP/$\beta_2$-mYFP transfectants. Soluble ICAM-1 (sICAM-1, residues 1–453) was expressed in CHO Lec 3.2.8.1 cells and purified as described in ref. 39. Before use, sICAM-1 was purified by using Superdex 200 (GE Healthcare, Pittsburgh, PA) permeation chromatography to ensure that it was monomeric.

**Flow Chamber Assay.** The flow chamber assay was performed as described in ref. 3. A polystyrene Petri dish to be used as the lower wall of the chamber was coated with a 5-mm-diameter, 20-$\mu$l spot of 10 $\mu$g/ml purified human ICAM-1/Fc$\gamma$ (R & D Systems, Minneapolis, MN) in coating buffer (PBS/10 mM $NaHCO_3$, pH 9.0) for 1 h at 37°C, followed by 2% human serum albumin in coating buffer for 1 h at 37°C to block nonspecific binding sites (3, 40). EDTA-prewashed cells were diluted to $1 \times 10^6$ per ml in $Ca^{2+}$- and $Mg^{2+}$-free Hanks' balanced salt solution/10 mM Hepes/0.5% BSA containing different divalent cations immediately before infusion in the flow chamber. Cells were allowed to accumulate for 30 s at 0.3 dyne·cm$^{-2}$ and for 10 s at 0.4 dyne·cm$^{-2}$. Then, shear stress was increased every 10 s from 1 dyne·cm$^{-2}$ up to 32 dyne·cm$^{-2}$ in 2-fold increments. The number of cells remaining bound at the end of each 10-s interval was determined. Rolling velocity at each shear stress was calculated from the average distance traveled by rolling cells in 3 s.

**FRET.** FRET was measured exactly as described in ref. 11. Cells ($10^6$ per ml) were washed and resuspended with 1 ml of L15 medium supplemented with 2.5% FCS and incubated in six-well plates with or without 1 mM $MnCl_2$/100 $\mu$g/ml sICAM-1 or 20 $\mu$g/ml $\alpha_L\beta_2$-activating mAb CBR LFA-1/2 at 37°C for 30 min. Then, cells were fixed with 3.7% formaldehyde/PBS for 10 min at room temperature.

**Cell Spreading and Microscopy.** Cell spreading assays were carried out in Delta T imaging chambers (Bioptechs, Butler, PA). The chambers were coated for 1 h at 37°C with 30 $\mu$g/ml protein A in coating buffer, followed by blocking with 1% BSA for 1 h at 37°C; then, they were coated with 20 $\mu$g/ml human ICAM-1–Fc$\gamma$ (from R & D Systems) in coating buffer for 1 h at 37°C. Transiently transfected 293T cells were detached with trypsin/EDTA, washed once with DMEM containing 0.5 mg/ml soybean trypsin inhibitor (Calbiochem, La Jolla, CA), and washed twice with DMEM. Cells were suspended in DMEM and seeded on ICAM-1–Fc$\gamma$-coated chambers. After incubation at 37°C for 2 h, cells were washed three times with PBS at pH 7.4 and fixed with 3.7% formaldehyde in PBS at room temperature for 5 min. The fixed cells were stained with phalloidin conjugated to Alexa Fluor 546 (Molecular Probes, Eugene, OR) after permeabilization with 0.05% Triton X-100 in PBS.

Differential interference contrast, interference-reflection microscopy, and fluorescence imaging was conducted on an Axiovert S200 epifluorescence microscope (Zeiss MicroImaging, Thornwood, NY) by using a ×63 oil objective coupled to an Orca CCD camera (Hamamatsu, Hamamatsu City, Japan). For the quantification of cell spreading, outlines of at least 100 adherent cells and cells in suspension (control) from randomly selected fields in each of three separate experiments were generated, and the number of pixels contained with each of these regions was measured by using OpenLab software (Improvision, Lexington, MA).

This work was supported by grants from the National Institutes of Health (HL48675 and CA31798 to T.A.S.) and the Arthritis Foundation (to C.V.C.).


1. Xiao, T., Takagi, J., Wang, J.-H., Coller, B. S. & Springer, T. A. (2004) *Nature* **432,** 59–67.
2. Xiong, J. P., Stehle, T., Zhang, R., Joachimiak, A., Frech, M., Goodman, S. L. & Arnaout, M. A. (2002) *Science* **296,** 151–155.
3. Chen, J. F., Salas, A. & Springer, T. A. (2003) *Nat. Struct. Biol.* **10,** 995–1001.
4. Chen, J. F., Takagi, J., Xie, C., Xiao, T., Luo, B.-H. & Springer, T. A. (2004) *J. Biol. Chem.* **279,** 55556–55561.
5. Mould, A. P., Barton, S. J., Askari, J. A., Craig, S. E. & Humphries, M. J. (2003) *J. Biol. Chem.* **278,** 51622–51629.
6. Shimaoka, M., Takagi, J. & Springer, T. A. (2002) *Annu. Rev. Biophys. Biomol. Struct.* **31,** 485–516.
7. Beglova, N., Blacklow, S. C., Takagi, J. & Springer, T. A. (2002) *Nat. Struct. Biol.* **9,** 282–287.
8. Shimaoka, M., Xiao, T., Liu, J.-H., Yang, Y., Dong, Y., Jun, C.-D., McCormack, A., Zhang, R., Joachimiak, A., Takagi, J., *et al.* (2003) *Cell* **112,** 99–111.
9. Takagi, J., Petre, B. M., Walz, T. & Springer, T. A. (2002) *Cell* **110,** 599–611.
10. Takagi, J., Strokovich, K., Springer, T. A. & Walz, T. (2003) *EMBO J.* **22,** 4607–4615.
11. Kim, M., Carman, C. V. & Springer, T. A. (2003) *Science* **301,** 1720–1725.
12. Lee, J.-O., Rieu, P., Arnaout, M. A. & Liddington, R. (1995) *Cell* **80,** 631–638.
13. Huang, C. & Springer, T. A. (1997) *Proc. Natl. Acad. Sci. USA* **94,** 3162–3167.
14. Salas, A., Shimaoka, M., Kogan, A. N., Harwood, C., von Andrian, U. H. & Springer, T. A. (2004) *Immunity* **20,** 393–406.
15. Salas, A., Shimaoka, M., Phan, U., Kim, M. & Springer, T. A. (2006) *J. Biol. Chem.* **281,** 10876–10882.
16. Shimaoka, M., Salas, A., Yang, W., Weitz-Schmidt, G. & Springer, T. A. (2003) *Immunity* **19,** 391–402.
17. Shimaoka, M. & Springer, T. A. (2004) *Curr. Top. Med. Chem.* **4,** 1485–1495.
18. Yang, W., Shimaoka, M., Salas, A., Takagi, J. & Springer, T. A. (2004) *Proc. Natl. Acad. Sci. USA* **101,** 2906–2911.
19. Marlin, S. D. & Springer, T. A. (1987) *Cell* **51,** 813–819.
20. Dransfield, I., Cabañas, C., Craig, A. & Hogg, N. (1992) *J. Cell Biol.* **116,** 219–226.
21. Mould, A. P., Akiyama, S. K. & Humphries, M. J. (1995) *J. Biol. Chem.* **270,** 26270–26277.
22. Lu, C., Ferzly, M., Takagi, J. & Springer, T. A. (2001) *J. Immunol.* **166,** 5629–5637.
23. Lu, C., Shimaoka, M., Zang, Q., Takagi, J. & Springer, T. A. (2001) *Proc. Natl. Acad. Sci. USA* **98,** 2393–2398.
24. Dransfield, I. & Hogg, N. (1989) *EMBO J.* **8,** 3759–3765.
25. Kamata, T., Tieu, K. K., Tarui, T., Puzon-McLaughlin, W., Hogg, N. & Takada, Y. (2002) *J. Immunol.* **168,** 2296–2301.
26. Bajt, M. L., Goodman, T. & McGuire, S. L. (1995) *J. Biol. Chem.* **270,** 94–98.
27. Huth, J. R., Olejniczak, E. T., Mendoza, R., Liang, H., Harris, E. A., Lupher, M. L., Jr., Wilson, A. E., Fesik, S. W. & Staunton, D. E. (2000) *Proc. Natl. Acad. Sci. USA* **97,** 5231–5236.
28. Alonso, J. L., Essafi, M., Xiong, J. P., Stehle, T. & Arnaout, M. A. (2002) *Curr. Biol.* **12,** R340–R342.
29. Harding, M. M. (2001) *Acta Crystallogr. D* **57,** 401–411.
30. Mould, A. P., Askari, J. A., Barton, S., Kline, A. D., McEwan, P. A., Craig, S. E. & Humphries, M. J. (2002) *J. Biol. Chem.* **277,** 19800–19805.
31. Mould, A. P., Barton, S. J., Askari, J. A., McEwan, P. A., Buckley, P. A., Craig, S. E. & Humphries, M. J. (2003) *J. Biol. Chem.* **278,** 17028–17035.
32. Luo, B.-H., Takagi, J. & Springer, T. A. (2004) *J. Biol. Chem.* **279,** 10215–10221.
33. Yang, W., Shimaoka, M., Chen, J. F. & Springer, T. A. (2004) *Proc. Natl. Acad. Sci. USA* **101,** 2333–2338.
34. Lu, C. & Springer, T. A. (1997) *J. Immunol.* **159,** 268–278.
35. Lu, C., Oxvig, C. & Springer, T. A. (1998) *J. Biol. Chem.* **273,** 15138–15147.
36. Petruzzelli, L., Maduzia, L. & Springer, T. A. (1995) *J. Immunol.* **155,** 854–866.
37. Robinson, M. K., Andrew, D., Rosen, H., Brown, D., Ortlepp, S., Stephens, P. & Butcher, E. C. (1992) *J. Immunol.* **148,** 1080–1085.
38. Martin, S., Casasnovas, J. M., Staunton, D. E. & Springer, T. A. (1993) *J. Virol.* **67,** 3561–3568.
39. Jun, C.-D., Carman, C. V., Redick, S. D., Shimaoka, M., Erickson, H. P. & Springer, T. A. (2001) *J. Biol. Chem.* **276,** 29019–29027.
40. de Chateau, M., Chen, S., Salas, A. & Springer, T. A. (2001) *Biochemistry* **40,** 13972–13979.
41. Xiong, J.-P., Stehle, T., Diefenbach, B., Zhang, R., Dunker, R., Scott, D. L., Joachimiak, A., Goodman, S. L. & Arnaout, M. A. (2001) *Science* **294,** 339–345.